



Mesoporous silica filled smart super oleophilic fibers of triblock copolymer nanocomposites for oil absorption applications

Yara Elgawady¹ · Deepalekshmi Ponnamma¹ · Samer Adham² · Mashael Al-Maas² · Ali Ammar³ · Karim Alamgir³ · Mariam Al Ali Al-Maadeed^{1,4} · Mohammad K. Hassan¹

Received: 21 March 2020 / Accepted: 28 May 2020 / Published online: 30 June 2020
© The Author(s) 2020

Abstract

Super oleophilic fibers of styrene-isoprene-styrene (SIS) block copolymer/mesoporous silica (MS) nanocomposites are fabricated by electrospinning, and their oil absorption efficiency is monitored by following two different approaches. The first way is by using the fibers as tubular packing materials for oil absorption, whereas the second approach uses the fibers as filtration membrane after deposition on the commercial polyethersulfone (PES) support. All composites are made by adding inorganic MS in different concentrations (2, 4, and 7 wt.%) to SIS block copolymer. The addition of MS increases the fiber diameters and leads to enlarged and bead-like appearances, especially at higher filler concentrations. The oil absorption efficiency is explored based on the oil absorption capacity of the samples as well as with the gravity-driven oil filtration experiments. The best oil absorption efficiency is achieved by the 4 wt.% SIS-MS composite (150% higher oil absorption capacity compared to the neat SIS), and it is used to spin on the PES mechanical support of different pore sizes (0.2 μ and 8 μ). Ultrafiltration tests conducted on those coated membranes observe improved oil rejection performance as the fibrous SIS-MS are layered on the commercial mechanical support.

Keywords Mesoporous · Fibrous membrane · Filtration · Oil-water separation · Superoleophilic

1 Introduction

Traditional separation of oil/water (O/W) emulsions face some challenges due to inadequate separation selectivity and the presence of residual oil in separated water and vice versa [1–3]. It is highly desirable to develop advanced membranes that can selectively absorb the oil from water [4]. Many polyester textiles, metal meshes, and polystyrene (PS)-based

materials selectively absorb or filter the oil. Such superhydrophobic or superoleophobic membranes satisfying both high speed and efficiency are widely investigated with additional advantages of self-cleaning, anti-fouling, recyclability, and no energy exhaustion [5]. The general approach of fabricating oil-water separating membranes involves designing superhydrophobic/superoleophilic membranes or superoleophobic/superhydrophilic materials [6]. Membrane-based separation has significant advantages of low chemical consumption, simplicity in design, and high quality water production [7–9], due to which it is the most industrially preferred method of oil separation.

Though many membrane fabrication methods exist, the technique of electrospinning is the most reliable method because of the uniform fiber production, possibility of nanosized fibers, and high aspect ratio of the produced fibers [10, 11]. Through electrospinning, sub-micron-sized fibers can form thin non-woven fiber mat or membranes with large surface area and small pores. Many investigations were conducted on this particular technique of membrane fabrication, and the materials were effective in the oil-water separation applications [12, 13]. Viswanadam et al. [14] fabricated

✉ Deepalekshmi Ponnamma
lekshmi_deepa@yahoo.com

✉ Mohammad K. Hassan
mohamed.hassan@qu.edu.qa

¹ Center for Advanced Materials, Qatar University, P. O. Box 2713, Doha, Qatar
² ConocoPhillips Global Water Sustainability Center, Qatar Science and Technology Park, Doha, Qatar
³ Department of Chemical and Biomolecular Engineering, University of Houston, Houston, TX 77204, USA
⁴ Materials Science and Technology Program, Qatar University, P. O. Box 2713, Doha, Qatar

polypropylene nanofiber filters in tubular geometry for the separation of water drops of 7–50 μm size from ultra-low sulfur diesel fuel with a face velocity of 1.55 cm/min. They also explained the dependence of fiber size, pore size, and surface roughness on surface hydrophobicity, and thus, its affinity towards [14]. Their results revealed that better performing tubular filter was able to separate water drops of 7 μm size when compared to the flat filters which could separate drops larger than 20 μm . Tai et al. reported [15] the fabrication of highly flexible and thermally stable electrospun nanofibers of carbon chains interpenetrated within 3D silica in which the concentration of silica was <27 wt.%. This ultra-hydrophobic membrane was mechanically strong and was able to withstand elevated temperatures up to 350 °C and a wide range of pH from 2 to 14. The surface roughness of electrospun fiber mats enhanced its hydrophobicity according to the Cassie-Baxter mechanism [16]. Smart surfaces with tunable oil wettability in response to external medium were also used to design intelligent membranes for industrial applications [17]. Electrospun membranes of PS/carbon nanotube (CNT) composite was used for gravity-driven oil-water separation experiments by our group [11]. Such membranes with a small concentration of CNT also exhibited antibacterial activity.

Many block copolymer (BCP) superhydrophobic smart surfaces studies are reported, consisting of polymer blocks of different physical and chemical properties, but covalently bonded [17–19]. Smart textiles with switchable superoleophilicity, superoleophobicity, and controllable oil/water separation capacity were made by grafting poly(2-vinylpyridine) and hydrophobic polydimethylsiloxane blocks by Zhang et al. [17]. Materials of switchable hydrophilicity/hydrophobicity were reported by blending amphiphilic copolymer additives with polymers such as polyvinylidene fluoride (PVDF), polysulfone, and polyethersulfone (PES) [20–22]. The hydrophobic/hydrophilic segment ratio can be controlled in such a way that the resulting ultrafiltration membranes possess tunable fouling resistance, flux response, and oil separation characteristics [23, 24]. Rajasekhar et al. synthesized an ABA type tri-block copolymer (TBC) of lateral pendant benzoic acid-polyacrylate blocks with PS central block by reversible addition-fragmentation chain transfer (RAFT) polymerization and used it for separating engine oil from an oil/water emulsion [23]. The membranes showed 2.5 times larger water flux, and maintained 99% oil rejection compared to the neat PVDF-based membrane.

Poly(styrene-isoprene-styrene) (SIS) is an unsaturated block copolymer of styrene with sufficient flexibility and softness, along with very good adhesive properties [25]. This thermoplastic elastomer is widely used in fabrication of adhesives and sealants. SIS composites were also used for manufacturing ultrafiltration membranes as described by Querelle et al. [26]. The variable molecular weights of this

polymer influence its dynamic properties and create micro-phase separation inside the polymer [27]. The self-assembling nature of this BCP is also observed in many solvents such as DMF and THF [28]. These specific behaviors can change their surface properties such as hydrophobicity and can be useful in separating oil from oil/water mixtures. Due to its elastomeric nature, the fiber formation by electrospinning is not extensively addressed for this BCP. Though the abovementioned studies report quite a lot information on various polymer-based membranes used for oil/water separation, commercial supports are widely applied for industrial oil/water separation.

Herein, smart electrospun fibers are fabricated from the SIS BCP with hydrophobic oil absorption performance. Mesoporous silica (MS) particles are added to strengthen the nanocomposite fibers to reach enhanced oil separation efficiency. Though, the improved oil adsorption capacity of MS when incorporated within BCP was previously reported by Fan et al. The specific use of MS in modifying the SIS BCP fiber interface is rather a new concept [29]. The surface morphology and contact angle studies performed here illustrate the feasible surface roughness and hydrophobicity of the electrospun fibers. The oil absorption capacity and the oil/water separability of the fibers are tested by three different ways. In the beginning, immersion in different oils is carried out to check the percentage of oil absorption by the SIS/MS fibers. Gravity-driven oil/water separation through tubular SIS/MS fiber roll-ups is analyzed based on the visual identification. The separation efficiency variation in the presence of different oils is explained based on relevant separation mechanisms. Ultrafiltration experiments are performed on SIS/MS fibers coated commercial PES supports under relevant industrial conditions targeting advanced produced water treatment technologies. Experiments were performed on a prepared synthetic produced water solution that mimics the characteristics of actual produced water.

2 Experimental techniques

2.1 Materials

The following materials were used to synthesize mesoporous silica: poly(ethylene glycol)-block-poly(propylene glycol)-block-poly(ethylene glycol) (EO20PO70EO20) (PEG-PPG-PEG, Pluronic® P-123) with an average molecular weight of (M_n) of ~5800 and tetraethyl orthosilicate (TEOS) (reagent grade 98%). The solvents, tetrahydrofuran (THF), dimethyl formamide (DMF), and all the abovementioned chemicals were obtained from Sigma-Aldrich and used as such without any further purification. The block copolymer (SIS) of density 0.92 g/cc consisting of 30% PS was purchased from KRATON D1165 PT (Kraton polymers). Three types of oil

in water mixtures were made using engine oil (density 0.910 kg/dm³ at 15 °C, purchased from Qatar lubricants company), olive oil (density 0.916 kg/L of Spanish origin), and coconut oil (density 0.92 kg/L of Indian origin).

2.2 Synthesis of mesoporous silica (SBA-15)

SBA-15 MS was synthesized using a sol-gel process with the aid of amphiphilic triblock copolymer, poly(ethylene glycol)-block-poly(propylene glycol)-block-poly(ethylene glycol) (EO20PO70EO20). In a solution consisting of 30 g of water and 120 g of 2 M HCl, 4 g of the amphiphilic triblock copolymer was dispersed, by magnetic stirring for 5 h. To this homogeneous solution, 9.5 g TEOS was added and stirred well, to result in a gel-like appearance. This gel was aged at 35–40 °C for 24 h, then heated to 100 °C for 18 h, and further cooled to room temperature. The precipitate was then washed with distilled water and ethanol to remove the copolymer, and left for 24 h to dry, followed by calcination at 550 °C for 6 h to decompose the triblock copolymer template [30].

2.3 Fabrication of SIS/mesoporous silica nanocomposites

SIS/MS nanocomposites were fabricated by the electrospinning technique, which ensured a decent distribution of MS nanoparticles in the SIS polymer [31]. The polymer was dispersed in a mixture of THF and DMF solvents in 4:1 ratio to make a 12% solution. This was done by magnetically stirring the SIS dispersion for 4 h at room temperature and at 800 rpm. Various concentrations of MS (2, 4, and 7 wt.%) were separately dispersed in the same solvent mixture in an ultrasonic bath for 1 h, and these dispersions were then added to the SIS solution. Overnight magnetic stirring was done for each SIS/MS nanocomposite suspensions to ensure maximum dissolution and homogeneity before the electrospinning process. The conditions of electrospinning were adjusted according to the SIS/MS concentration, as illustrated in Table 1. It was observed that the MS concentration highly influenced the viscosity of SIS dispersion, and fibers were not formed under the same applied voltage and solution flow rate.

Table 1 Electrospinning conditions applied for spinning the various SIS/MS dispersions

Samples code	Flow rate (ml/h)	MS concentration (%)	Voltage (kV)
Neat SIS	1	0	10
SIS/MS2	1.8	2	12
SIS/MS4	2.5	4	15
SIS/MS7	3	7	16.5

2.4 Characterization techniques

Morphology of MS and the SIS/MS nanocomposite fibers was observed by scanning electron microscopy (SEM) images using JSM Jeol 6610 microscope at an accelerated voltage of 15 kV. Fiber samples were sputtered with a thin layer of gold before the SEM analysis. For the transmission electron microscope (TEM) images, the Philips CM200 TEM employing an accelerating voltage of 200 kV was used. Small-angle X-ray scattering (SAXS) studies were performed during the wave vector range $0.007 \text{ }^\circ\text{A}^{-1} < Q < 0.3 \text{ }^\circ\text{A}^{-1}$ on a Rigaku S-MAX3000 beamline. Wide-angle X-ray diffraction (WAXD) patterns of the samples were recorded by a Philips diffractometer using Cu K α radiation ($\lambda = 1.5418 \text{ \AA}$) at 40 kV and 40 mA. The effect of increasing the MS concentration in the composite's thermal degradation behavior was tested using a Perkin-Elmer TGA 4000 thermogravimetric analyzer (TGA). Oil and water contact angles for different samples were compared using a Data physics contact angle goniometer. Measurements were done at five different places for the same sample surface and average value was taken. Oil-water separation was conducted using different techniques of oil absorption and gravity-driven oil filtration to determine the most optimum concentration for the best separation outcomes, as illustrated below.

2.4.1 Oil absorption capacity test

Oil absorption capacity test was performed for all the samples using different types of oil. The procedure was as follows. Specific amount of the prepared sample sheet was immersed separately in a series of 3 ml engine oil, coconut oil, and olive oil for 60 min. The samples were then removed and subjected to a steady flow of warm air for 30 s to get rid of excess oil on the surface. Subsequently, the sample was re-weighed, and the percentage increase in the sample's weight was calculated using the following formula, where W_2 is the final weight and W_1 is the initial weight of the samples, respectively, after and before the oil absorption.

$$\% \text{increase} = \left(\frac{W_2 - W_1}{W_1} \right) 100 \quad (1)$$

2.4.2 Gravity-driven oil filtration

An oil/water mixture of 20 ml was made by mixing 18 ml water and 2 ml oil, by ultrasonication for 3 h. Then, the electrospun fiber was cut into smaller equal-sized pieces (1 cm²), which were then rolled into cylindrical shapes [14], as seen in Fig. 1. Around 20 such pieces were closely stacked into a funnel through which the oil-water mixture was allowed

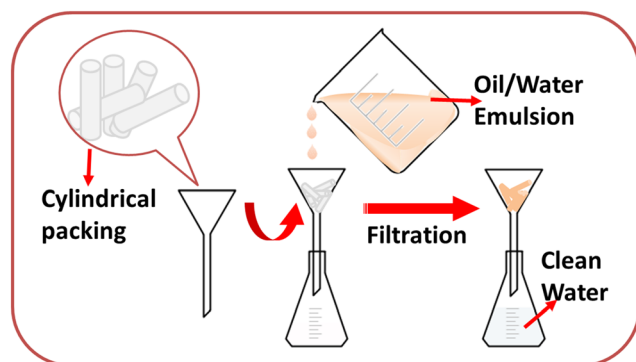


Fig. 1 Schematic illustration of the rolled cylindrical shapes and the gravity-driven oil/water filtration

to pass. Finally, pure water was collected from the flask kept under the funnel.

2.4.3 Ultrafiltration test setup and protocol

As shown in Fig. 2, the ultrafiltration bench scale setup includes a 50 ml Amicon stirred cell (Millipore, USA) having an active filtration area of 13.4 cm^2 and the capability of testing flat sheet membranes at various pressures. A 3-L feed reservoir was pressurized using compressed nitrogen to provide pressure reaching up to 5 bar to the Amicon cell. To accurately measure the applied pressure, a pressure transducer (PX309, Omega Engineering, USA) was installed between the reservoir outlet and the Amicon cell. The cell was placed on a stir plate (Sterlitech, USA) to ensure the homogeneity of the feed solution. For data collection and processing, the unit stores the experimental data through a LabVIEW (cRIO-9035, National Instruments, USA) acquisition system.

Ultrafiltration tests were conducted on the commercial $8 \mu\text{m}$ PES support (Sterlitech, USA) and the SIS/MS4-coated PES membrane. First, both membranes were initially soaked overnight in deionized water before testing. Then, each membrane was compacted using 1–2 L of deionized water as the feed solution at a pressure of 0.5 bar, magnetic

stirring speed of 560 rpm, and a run time of approximately 30–40 min until obtaining stable flux measurements. After that, a synthetically produced water solution having a total organic carbon (TOC) concentration ranging between 22 and 26 mg/L was prepared using actual crude oil sourced from ConocoPhillips' operations and used for the oil-water separation test that was carried out at similar test conditions while targeting a 50% feed volume reduction. To assess oil rejection, samples of the feed and permeate were collected for TOC measurements using the TOC Analyzer (TOC-V, Shimadzu, Japan).

3 Results and discussion

3.1 Morphology and structural analysis of mesoporous silica

The typical sol-gel process results in disc shape particles of MS [32] as shown in Fig. 3a. SEM image given in Fig. 3b observes the average size of such platelet-like/disc-like MS particles as 800 nm. High-resolution transmission electron microscope (HRTEM) image of the nanoparticle shows the ordered crystalline lattice as represented in Fig. 3c. Parallel lines with wide spacing correspond to the elongated ellipsoid structural information for the synthesized MS particles [33]. The FTIR (Fig. 3d) and XRD (Fig. 3e) patterns give the structural information of MS nanoparticles.

The FTIR spectra are similar to the reported bands of SiO_2 nanoparticles. The bands at $\sim 802 \text{ cm}^{-1}$ and 1097 cm^{-1} in the FTIR curve (Fig. 3d) attribute to the asymmetric stretching and bending vibrations of Si–O–Si bonds in the SiO_2 structure, respectively [34]. The X-ray diffraction curve (Fig. 3e) further offers evidence for the formation of silica nanoparticles with an excellent crystalline structure. This can be confirmed by the plot of synthesized MS nanoparticles that shows an intense peak at $2\theta = 24^\circ$ corresponding to the SiO_2 peak. As reported

Fig. 2 Amicon cell ultrafiltration unit diagram—GWSC's laboratory

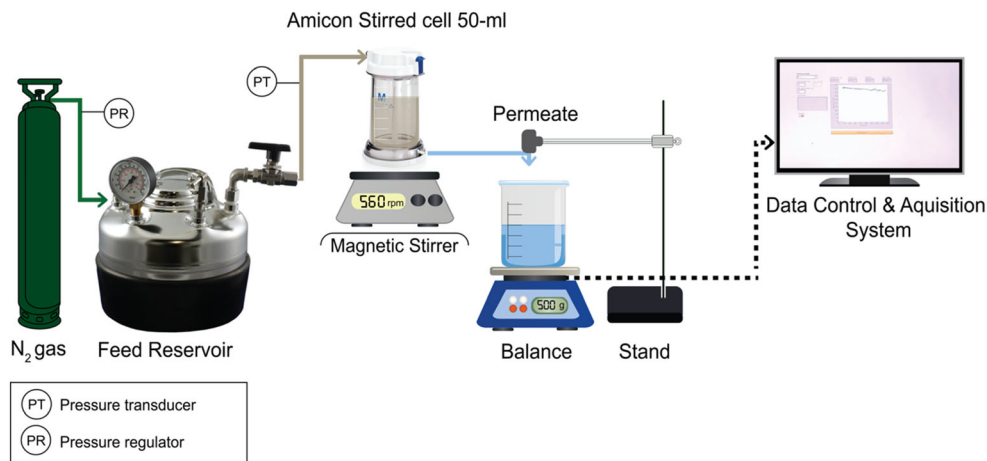
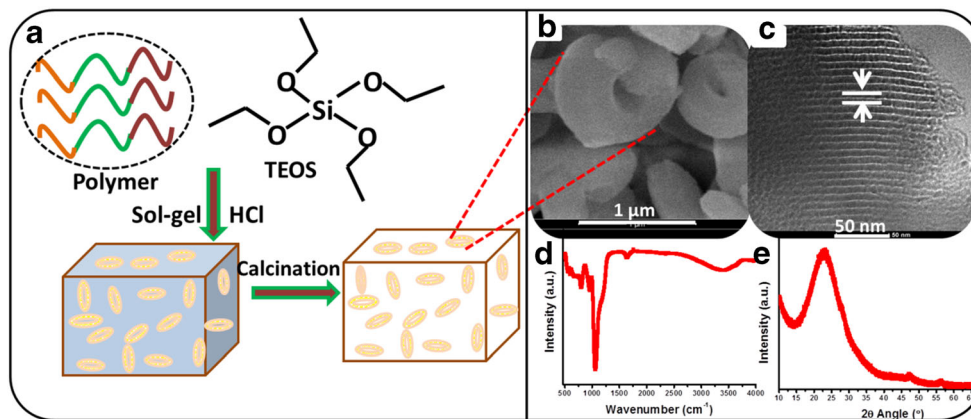


Fig. 3 a Schematic representation of the synthesis of MS. b SEM image. c HRTEM image d) FTIR spectrum. e XRD pattern for the MS nanoparticles



by Sharmiladevi et al. [35], this can be attributed to the effect of the smaller particle size of the nanoparticles.

3.2 Morphology and structural analysis of SIS/mesoporous silica electrospun fibers

Electrospinning was used to synthesize the samples as it is a simple and low-cost method [36]. Different concentrations of MS (2, 4, and 7 wt.%) were added to the SIS block copolymer to obtain various composite samples, the SEM images of which are represented in Fig. 4. The fibrous structure of SIS was greatly affected by the incorporation of MS particles [37], as can be seen from Fig. 4a–d. There is an apparent change in the fiber diameter as MS particles are incorporated in the SIS polymer (fiber diameters were calculated using the ImageJ software and 25 measurements were taken for each sample). In the neat SIS, the average fiber diameter was about $0.50 \pm 0.15 \mu\text{m}$, which is enhanced to $0.79 \pm 0.17 \mu\text{m}$ as the MS (SIS/MS2) was added to it. For the SIS/MS4 and SIS/

MS7, the calculated diameters were $0.89 \pm 0.3 \mu\text{m}$ and $1.50 \pm 0.40 \mu\text{m}$, respectively. The presence of larger clusters/aggregates due to the enhanced MS concentration is also evident in these composites, especially at 7 wt.% of MS. A close observation about the fibrous structure (SIS/MS4 composite) is done by the TEM technique as represented in Fig. 4e, the inset of which shows the MS single-particle structure, by TEM. It is clear that the MS particle is dispersed in the SIS fiber, which is a probable reason for the thicker fiber appearances (with a fiber diameter of approximately $0.98 \mu\text{m}$), as observed from the TEM. As obvious from the morphologies, the bulkiness of the fibers increases proportionally with the MS concentration, which is also reported elsewhere [38].

Figure 5 addresses the structural details of the SIS/MS nanocomposites employing XRD and FTIR studies. Figure 5a shows the SAXS patterns for the MS particles, neat SIS, and the SIS/MS4 nanocomposite. The highly intense peak observed in the figure for the MS corresponds to the (100) reflection for the two-dimensional cylindrical structure

Fig. 4 SEM images of a neat SIS, b SIS/MS2, c SIS/MS4, and d SIS/MS7 nanocomposites and e TEM image of the SIS/MS4 composite; the inset shows the TEM image of a single MS

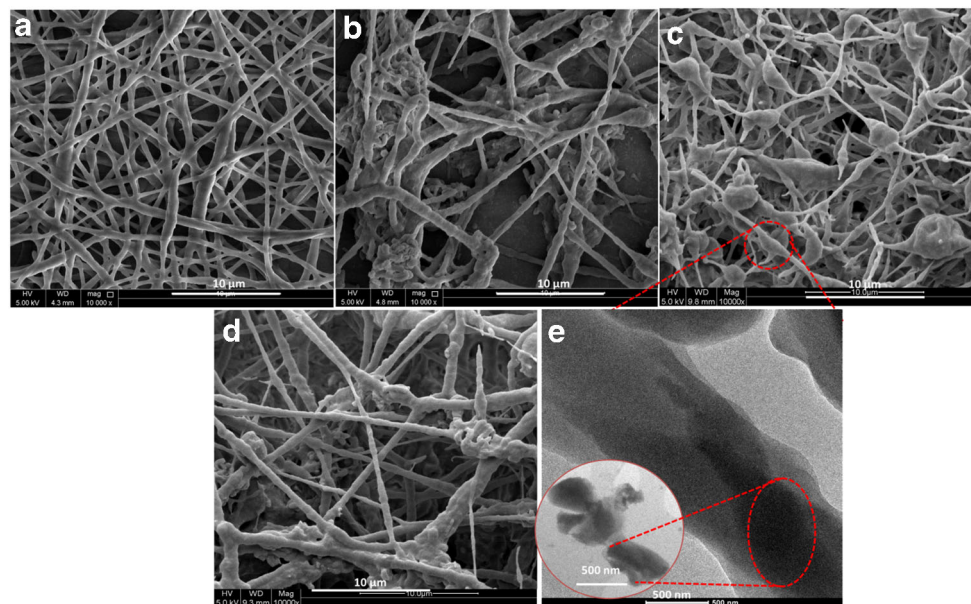
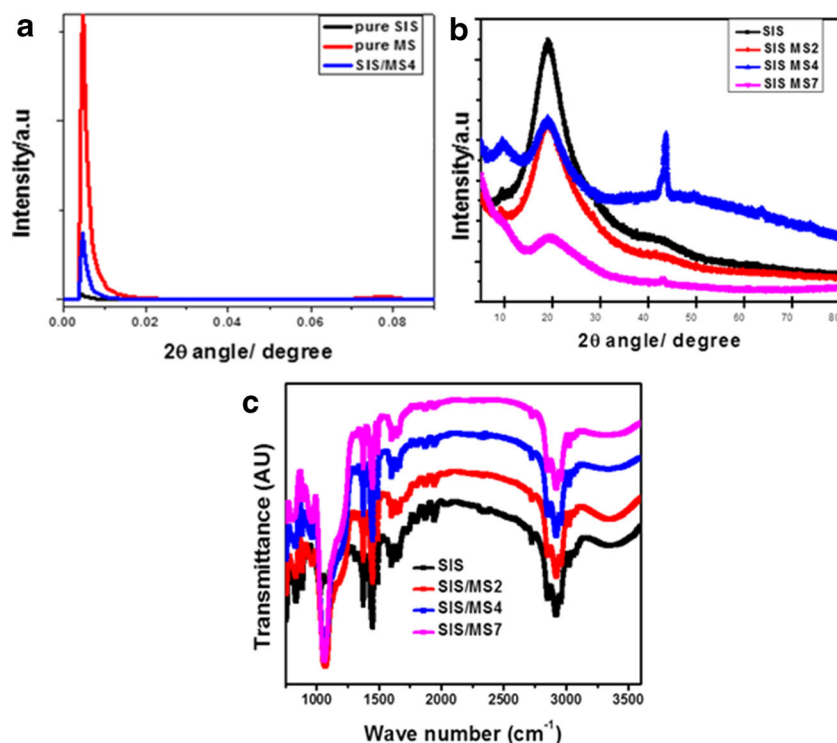


Fig. 5 **a** SAXS pattern, **b** WAXD pattern, and **c** FTIR spectra for the neat SIS and its nanocomposites with MS



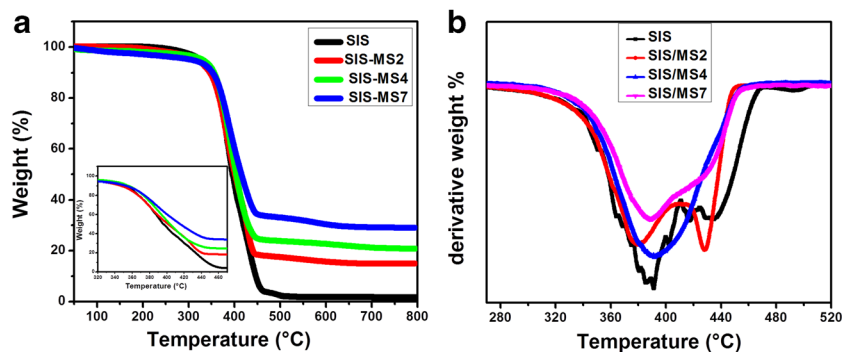
of hexagonal lattice [39]. This is also present in the SIS/MS4 composite, but with lesser intensity, probably due to the presence of MS in smaller concentration and reinforcement within the SIS chains. However, the peak does not appear in neat SIS. The WAXD in Fig. 5b for the neat SIS fibers and different concentrations of SIS/MS nanocomposites show broad diffuse peaks confirming the presence of crystalline silica particles. The broad peak around 19° is attributed to the presence of SIS polymer and its amorphous nature [40]. The small peak below 10° is related to the MS particles, and its intensity becomes higher as the MS concentration increases. A higher order reflection peak is observed around 41° for the composites (more clearly in SIS/MS4), due to the well-distributed MS in the SIS medium [41]. For all other samples, this peak was less clear. Figure 5c shows the FTIR transmission spectra of neat SIS fibers and the various SIS/MS nanocomposites in the 400–4000 cm^{-1} range, recorded at room temperature. The transmission band at 1090 cm^{-1} corresponds to the asymmetric vibration of Si–O bond, the band at 950 cm^{-1} is attributed to asymmetric vibration of Si–OH bond, and the peak at 795 cm^{-1} arises from the symmetric vibration of Si–O bond in SIS/MS nanocomposites. All peak intensities were obviously enhanced as the MS concentration increases in the composite, which confirms its presence with the corresponding concentrations. We can describe the transmission bands between 800 and 1260 cm^{-1} as a superimposition of various SiO_2 peaks, Si–OH bonding, and peaks from residual organic groups as well. The bands at 2980 cm^{-1} ($-\text{CH}_3$) and

2930 cm^{-1} ($-\text{CH}_2$) can be attributed to the existence of some unreacted TEOS in the silica particles, as reported by Aldona et al. [42].

3.3 Thermal stability of the SIS/MS nanocomposites

Thermogravimetric analysis (TGA) was done by heating the samples from room temperature to 800°C at a constant rate of $10^\circ\text{C}/\text{min}$. As shown in Fig. 6a, all samples are thermally stable up to 300°C , and then starts to degrade afterward. This weight loss is attributed to the thermal decomposition of the carbon chains within the SIS polymer. The incorporation of MS at different concentrations in SIS/MS nanocomposites clearly improves the stability of the composites [43–45]. As indicated in Fig. 6b, the SIS block copolymer has a multiple degradation behavior due to its amorphous nature and the presence of isoprene and styrene contents in the skeleton. This trend is the same for SIS/MS2 composite due to the smaller amount of nanoreinforcement. However, the MS stabilizes the polymer chains as the multiple peaks are observed to be merged at the higher concentrations of MS particles. This ensures the thermally stabilizing nature of MS nanoparticles and the perfect single degradation peak observed for the SIS/MS4 composite concludes its maximum thermal stability [46, 47]. At higher concentration (SIS/MS7), the MS particles form clusters and destabilize the system, so that the degradation for SIS starts to appear.

Fig. 6 **a** Thermogravimetric and **b** derivative thermogravimetric curves for the SIS/MS nanocomposites



3.4 Surface property analysis of SIS nanocomposites

Contact angle studies for all SIS/MS nanocomposite samples were done using various media such as water, olive oil, coconut oil, and engine oil. The resulting values are provided in Table 2. The aqueous contact angle was $133.5^\circ \pm 3$, for the neat polymer whereas it is enhanced to $142.1^\circ \pm 1$ for the SIS/MS 4 wt.% composite. The increase in the hydrophobicity is due to the presence of MS in the optimum concentration [43]. The contact angles for the SIS/MS2 and SIS/MS4 followed a regular trend, according to the concentration of MS and its distribution within the polymer chains. However, a higher concentration of MS at 7 wt.% decreases the contact angle, due to the agglomerated MS particles within the SIS medium. All contact angle values were taken as the oil drops immediately falls on the spun fibers and also after 10 s of oil penetration. In most of the cases, the oil penetrates so quickly and the fibers behave as superoleophilic fibers. The contact angle images provided in the table show clear evidence for the oil penetration. Among all the composites, the SIS/MS4 showed the best oil absorption performance. When compared with coconut and olive oils, the engine oil exhibited consistent and stable oil-absorbing performance; therefore, this particular oil was used for the gravity-driven oil filtration experiments.

3.5 Influence of temperature and humidity on the samples' structure and contact angle

The effect of humidity and temperature on the oil absorption performance of the SIS/MS4 nanocomposite was studied to mimic the real environmental conditions of the typically produced water from petrochemical industries. Samples and the oil/water mixture were exposed to relatively high temperature and humidity conditions (temperature of 50°C and 80% humidity, each at a time) for 15 min, to simulate actual conditions in the petroleum industry in Qatar. Figure 7 a and b show no specific effect on the contact angles of water and oil drops when exposed to temperature and humidity conditions by the SIS/MS4 composite fibers. The data obtained were compared with the above results taken in the lab environment. In addition, the crystallinity influence of the fibers if exposed to

higher temperatures is also investigated by XRD, as given in Fig. 7c. Both peaks in the XRD spectra appear similar for the composites before and after temperature treatment with no shifts in peak position.

3.6 Investigating the oil absorption for the SIS/MS nanocomposites

3.6.1 Oil absorption capacity measurements









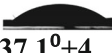


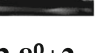








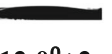











The samples were cut and immersed in various oils—coconut, olive, and engine oils—for 60 min for achieving maximum oil absorption (Fig. 8a). Later, the fibers were dried and weighed to calculate the percentage of oil absorption as per Eq. 1. The images of the samples before and after oil absorption are provided in Fig. 8a. The percent of oil absorption, Fig. 8b, indicates an increase in oil absorption capacity for the composites with increasing the amount of MS nanoparticles up to 4 wt.%, then drops afterward. This evidences that the 4 wt.% is the optimum concentration in which the oil absorption is the maximum, and after that, the fiber is not able to absorb more oil. The reason for the reduction in oil absorption could be attributed to the agglomeration of the MS nanoparticles beyond the 4 wt.% concentration, and thereby the loss of hydrophobicity of the fibers.

3.6.2 Gravity-driven oil filtration studies using tubular fiber packings

Gravity-driven oil absorption experiments were conducted using a mixture of engine oil/water as shown in Fig. 9. The separating funnel is packed with tubular roll-ups of the SIS/MS4 samples (inset of Fig. 9a), and the oil/water mixture is allowed to pass through it (Fig. 9b). As soon as the mixture passes through the packed funnel, the oil gets absorbed on the fiber packings allowing the water to come out to the bottom of the funnel (Fig. 9c). After the oil has been absorbed, the packings are fully covered with the oil (Fig. 9d).

The tubular shapes of the fibers increase the surface area so that more oil droplets could get absorbed by the packings [14].

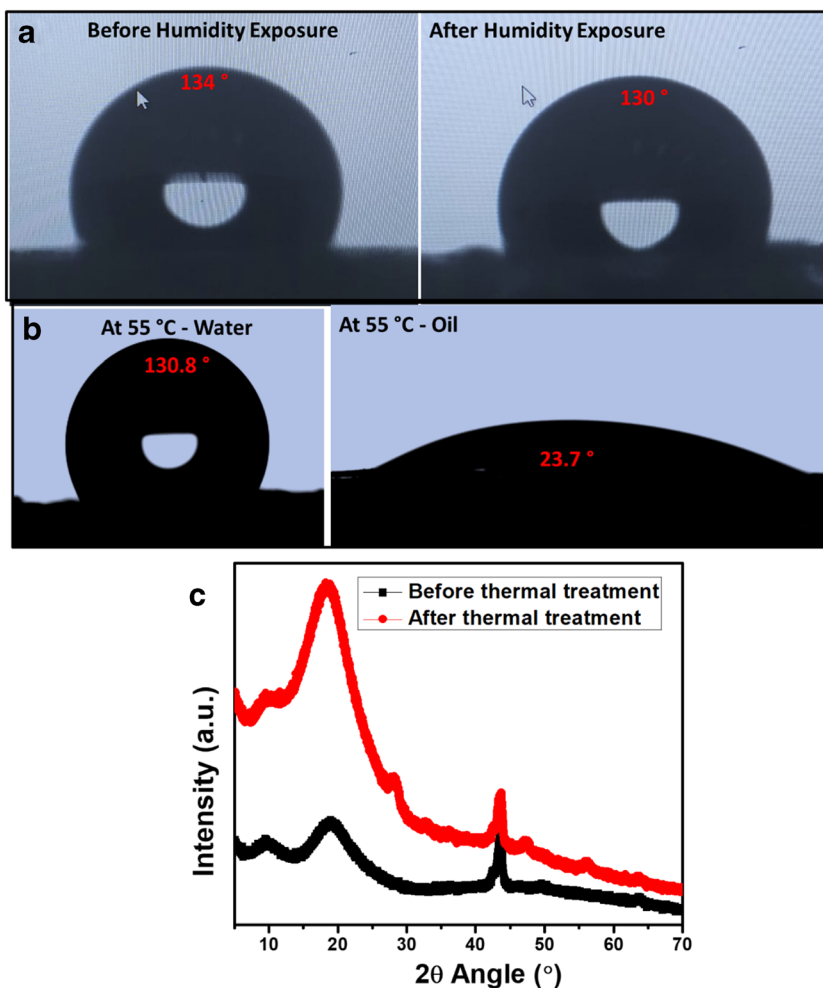
Table 2 Water and oil contact angle values for various SIS/MS nanocomposites

		SIS	SIS/MS 2	SIS/MS 4	SIS/MS7
Water	Immediate	 133.5 ⁰ ±3	 141.0 ⁰ ±3	 142.1 ⁰ ±1	 135.8 ⁰ ±1
	After 10 s	 131.0 ⁰ ±3	 139.7 ⁰ ±3	 140.0 ⁰ ±1	 134.8 ⁰ ±1
Olive oil	Immediate	 37.1 ⁰ ±4	 28.4 ⁰ ±1	 12.6 ⁰ ±4	 32.8 ⁰ ±2
	After 10 s	 19.2 ⁰ ±4	 Flat	 5.0 ⁰ ±4	 6.6 ⁰ ±2
Engine oil	Immediate	 32.4 ⁰ ±2	 25.2 ⁰ ±2	 29.4 ⁰ ±2	 27.9 ⁰ ±2
	After 10 s	 12.0 ⁰ ±2	 8.1 ⁰ ±2	 6.3 ⁰ ±2	 flat
Coconut oil	Immediate	 17.0 ⁰ ±2	 14.5 ⁰ ±3	 15.8 ⁰ ±1	 25.9 ⁰ ±1
	After 10 s	 6.6 ⁰ ±2	 flat	 6.5 ⁰ ±1	 6.0 ⁰ ±3

The water drops are repelled by the cylindrical packings and thus moves down through the funnel. The water drops roll over the hydrophobic fiber packings, and accumulates at the

bottom of the flask. The experiments of oil filtration were repeated three times, and a maximum of 6 ml oil was absorbed by the 20 pieces of tubular fiber packings.

Fig. 7 Effect of **a** humidity and **b** temperature on the contact angle values of the SIS/MS4 nanocomposite. **c** XRD spectra of SIS/MS4 before and after heat treatment



3.6.3 Ultrafiltration test

Ultrafiltration tests were initially conducted on the commercial 8 μm PES support that has been used as the performance benchmark for the SIS/MS4-coated PES membrane. Membranes were both compacted at a pressure of 0.5 bar using deionized water as the feed solution, until reaching stable water flux rates. Those rates obtained under the

abovementioned test conditions are referred to as the clean membrane flux rates and are normalized by the applied pressure, as presented in Fig. 10. The figure shows the impact on the commercial 8 μm PES support specific flux rate after layering the SIS/MS4 coating. The SIS/MS4 layer has caused a drop of approximately 35% in the commercial 8 μm PES support specific flux rate from 28,616 to 18,555 (L/m² h)/bar. For the oil rejection evaluation, both membranes were tested

Fig. 8 **a** Testing setup for the oil absorption capacity by the SIS/MS4 composite in various oils—coconut oil, olive oil, and engine oil. **b** Oil absorption capacity for samples with variable concentrations of MS nanoparticles

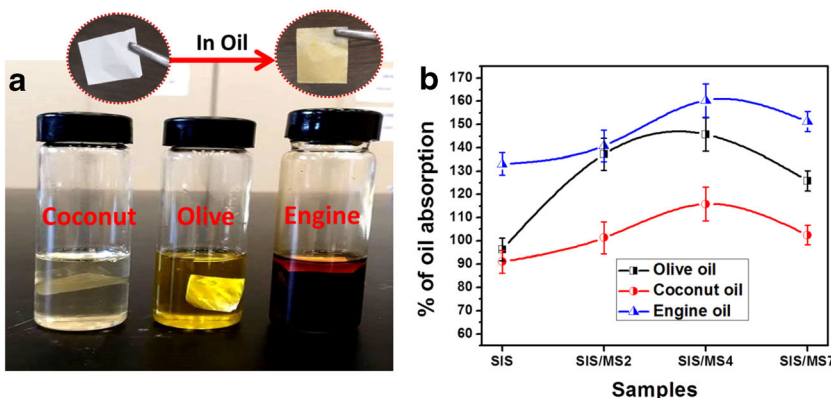
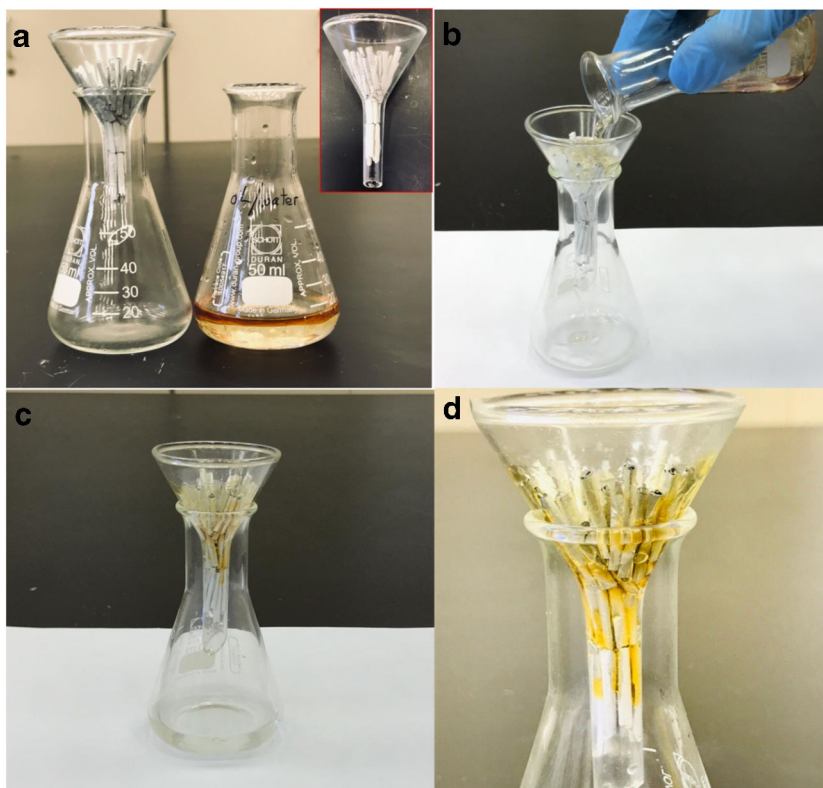


Fig. 9 Gravity-driven oil absorption experiment. **a** The setup used with the tubular fiber packings in the inset. **b** Pouring oil/water mixture. **c** Gravity-driven separation. **d** The absorbed oil by the fiber packings



using the synthetic produced water solution having an initial TOC concentration ranging between ≈ 22 – 26 mg/L [48]. Tests were carried out using a feed solution volume of 100 ml, and 50 ml of permeate was collected at the end of the filtration test, i.e., 50% volume reduction. Testing both membranes on the synthetically produced water solution has resulted in a decrease of around 23% and 31% in the specific flux rates for the commercial $8\ \mu\text{m}$ PES support, and the SIS/MS4-coated PES membrane respectively which implies that both membranes got fouled. TOC measurements on collected samples of the feed and permeate from the oil rejection tests conducted on both membranes are presented in Table 3. A TOC removal percentage of $\approx 63\%$ was achieved by the commercial $8\ \mu\text{m}$ PES support, whereas a rejection of $\approx 80\%$ was

obtained by the SIS/MS4-coated PES membrane. Thus, the SIS/MS4 coating has improved the oil rejection performance of the commercial $8\ \mu\text{m}$ PES support.

4 Conclusions

Oleophilic SIS/MS nanocomposites were fabricated by electrospinning process, and the nanoparticle concentration was optimized based on the morphology and contact angle values. The SIS/MS composites were made in the form of cylindrical packings as well as membranes deposited on PES support for enhancing their oil absorption performances. The gravity-driven oil absorption experiments and the oil absorption studies showed the ability of the SIS/MS composite at 4 wt.% of the MS particles in selectively absorbing the oil molecules. Various compositions of SIS/MS composites were fabricated, and we found that maximum oil separation efficiency was achieved at 4 wt.% of disc-shaped MS

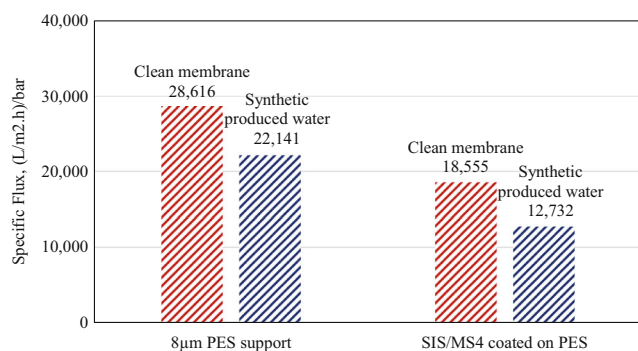


Fig. 10 Ultrafiltration—test results on the commercial $8\ \mu\text{m}$ PES support and the SIS/MS4-coated PES membrane

Table 3 Ultrafiltration tests—TOC results

	Commercial $8\ \mu\text{m}$ PES membrane	SIS/MS4-coated PES membrane
Feed (mg/L)	22	26
Permeate (mg/L)	8.1	5.3
TOC removal%	63%	80%

nanoparticles. In this particular composite, the oil absorption capacity was increased by 160.3% and the aqueous contact angle was increased from 133.5° for the neat SIS to 142.1° revealing maximum hydrophobicity as well. Stability of the oil separation by the tubular packings was confirmed by exposing to a higher temperature (50 °C) and humidity (80%) to mimic operation conditions in the oil/gas industry. Ultrafiltration tests conducted on the commercial 8 µm PES support and the SIS/MS4-coated PES membrane using a synthetic produced water solution showed that the application of SIS/MS4 coating had improved the oil rejection of the PES support. These properties, along with higher thermal stability, make the SIS/MS fibers suitable candidates for filtering oil molecules from industrial produced water.

Acknowledgments This publication is made possible by NPRP grant 10-0127-170269 from the Qatar National Research Fund (a member of Qatar Foundation). The statements made herein are solely the responsibility of the authors. The authors would like to thank the Qatar University' Central Laboratories Unit (QUCLU) for their assistance with the SEM and TEM measurements of the samples. In addition, we thank Dr. Arnold Janson and Mr. Joel Minier Matar, GWSC, ConocoPhillips, for their assistance throughout some of the experiments and with the manuscript revisions.

Funding Information Open Access funding provided by the Qatar National Library.

Compliance with ethical standards

Conflict of interest The authors declare that they have no conflict of interest.

Open Access This article is licensed under a Creative Commons Attribution 4.0 International License, which permits use, sharing, adaptation, distribution and reproduction in any medium or format, as long as you give appropriate credit to the original author(s) and the source, provide a link to the Creative Commons licence, and indicate if changes were made. The images or other third party material in this article are included in the article's Creative Commons licence, unless indicated otherwise in a credit line to the material. If material is not included in the article's Creative Commons licence and your intended use is not permitted by statutory regulation or exceeds the permitted use, you will need to obtain permission directly from the copyright holder. To view a copy of this licence, visit <http://creativecommons.org/licenses/by/4.0/>.

References

1. D. Ponnamma, K.K. Sadasivuni, S. Thomas, I. Krupa, M.A. AlMa'adeed, Flexible oil sensors based on multiwalled carbon nanotube-filled isoprene elastomer composites. *Rubber Chem. Technol.* **89**(2), 306–315 (2016)
2. M. Laad, D. Ponnamma, K.K. Sadasivuni, *Int. J. Appl. Eng. Res.* **12**(11), 2855 (2017)
3. Z. Chu, Y. Feng, S. Seeger, Oil/water separation with selective superantwetting/superwetting surface materials. *Angewandte Chem. Int. Ed.* **54**(8), 2328–2338 (2015)
4. J. Gu, P. Xiao, J. Chen, F. Liu, Y. Huang, G. Li, J. Zhang, T. Chen, Robust preparation of superhydrophobic polymer/carbon nanotube hybrid membranes for highly effective removal of oils and separation of water-in-oil emulsions. *J. Mat. Chem. A.* **2**(37), 15268 (2014)
5. L. Feng, Z. Zhang, Z. Mai, Y. Ma, B. Liu, L. Jiang, D. Zhu, A super-hydrophobic and super-oleophilic coating mesh film for the separation of oil and water. *Angewandte Chem.* **116**(15), 2046–2048 (2004)
6. B. Wang, W. Liang, Z. Guo, W. Liu, Biomimetic super-lyophobic and super-lyophilic materials applied for oil/water separation: a new strategy beyond nature. *Chem. Soc. Rev.* **44**(1), 336–361 (2015)
7. A. Janson, J. Minier-Matar, E. Al-Shamari, A. Hussain, R. Sharma, D. Rowley, S. Adham, Evaluation of new ion exchange resins for hardness removal from boiler feedwater. *Emerg. Mat.* **1**(1–2), 77–87 (2018)
8. A. Nagaraj, D. Govindaraj, M. Rajan, Magnesium oxide entrapped polypyrrole hybrid nanocomposite as an efficient selective scavenger for fluoride ion in drinking water. *Emerg. Mat.* **1**(1–2), 25–33 (2018)
9. N. Abdullah, N. Yusof, A.F. Ismail, F.E. Othman, J. Jaafar, L.W. Jye, W.N. Salleh, F. Aziz, N. Misdan, Effects of manganese(VI) oxide on polyacrylonitrile-based activated carbon nanofibers (ACNFs) and its preliminary study for adsorption of lead(II) ions. *Emerg. Mat.* **1**(1–2), 89–94 (2018)
10. H. Parangusan, D. Ponnamma, M.A. Al-Maadeed, Stretchable electrospun PVDF-HFP/Co-ZnO nanofibers as piezoelectric nanogenerators. *Sci. Rep.* **8**(1), 754 (2018)
11. H. Parangusan, D. Ponnamma, M.K. Hassan, S. Adham, M.A. Al-Maadeed, Designing carbon nanotube-based oil absorbing membranes from gamma irradiated and electrospun polystyrene nanocomposites. *Materials.* **12**(5), 709 (2019)
12. X. Wang, J. Yu, G. Sun, B. Ding, Electrospun nanofibrous materials: a versatile medium for effective oil/water separation. *Mat. Today.* **19**(7), 403–414 (2016)
13. F.E. Ahmed, B.S. Lalia, N. Hilal, R. Hashaikeh, Underwater superoleophobic cellulose/electrospun PVDF-HFP membranes for efficient oil/water separation. *Desalination.* **344**, 48–54 (2014)
14. G. Viswanadam, G.G. Chase, Water-diesel secondary dispersion separation using superhydrophobic tubes of nanofibers. *Separation Purification Technol.* **104**, 81–88 (2013)
15. M.H. Tai, P. Gao, B.Y. Tan, D.D. Sun, J.O. Leckie, Highly efficient and flexible electrospun carbon-silica nanofibrous membrane for ultrafast gravity-driven oil-water separation. *ACS Appl. Mat. Interf.* **6**(12), 9393–9401 (2014)
16. A.B. Cassie, S. Baxter, *Transactions of the Faraday Society* **40**, 546 (1944)
17. L. Zhang, Z. Zhang, P. Wang, *NPG Asia Mat.* **4**(2), 8 (2012)
18. S. Kumar, Y.L. Dory, M. Lepage, Y. Zhao, Surface-grafted stimuli-responsive block copolymer brushes for the thermo-, photo- and ph-sensitive release of dye molecules. *Macromolecules.* **44**(18), 7385–7393 (2011)
19. I. Luzinov, S. Minko, V.V. Tsukruk, Responsive brush layers: from tailored gradients to reversibly assembled nanoparticles. *Soft Matt.* **4**(4), 714 (2008)
20. B. Xue, L. Gao, Y. Hou, Z. Liu, L. Jiang, Temperature controlled water/oil wettability of a surface fabricated by a block copolymer: application as a dual water/oil on-off switch. *Adv. Mat.* **25**(2), 273–277 (2013)
21. H. Li, X. Zhao, P. Wu, S. Zhang, B. Geng, Facile preparation of superhydrophobic and superoleophilic porous polymer membranes for oil/water separation from a polyarylester polydimethylsiloxane block copolymer. *J. Mat. Sci.* **51**(6), 3211–3218 (2016)
22. J.J. Li, L.T. Zhu, Z.H. Luo, Electrospun fibrous membrane with enhanced swithchable oil/water wettability for oily water separation. *Chem. Eng. J.* **287**, 474–481 (2016)
23. T. Rajasekhar, M. Trinadh, P.V. Babu, A.V. Sainath, A.V. Reddy, Oil-water emulsion separation using ultrafiltration membranes

- based on novel blends of poly(vinylidene fluoride) and amphiphilic tri-block copolymer containing carboxylic acid functional group. *J. Membr. Sci.* **481**, 82–93 (2015)
24. E.A. Jackson, M.A. Hillmyer, Nanoporous membranes derived from block copolymers: from drug delivery to water filtration. *ACS Nano* **4**(7), 3548–3553 (2010)
 25. K.K. Sadasivuni, D. Ponnamma, P. Kasak, I. Krupa, M.A. Al-Maadeed, Designing dual phase sensing materials from polyaniline filled styrene–isoprene–styrene composites. *Mat. Chem. Phys.* **147**(3), 1029–1036 (2014)
 26. S.E. Querelle, E.A. Jackson, E.L. Cussler, M.A. Hillmyer, Ultrafiltration membranes with a thin poly(styrene)-b-poly(isoprene) selective layer. *ACS Appl. Mater. Interfaces* **5**(11), 5044–5050 (2013)
 27. P. Georgopoulos, U.A. Handge, C. Abetz, V. Abetz, Influence of block sequence and molecular weight on morphological, rheological and dielectric properties of weakly and strongly segregated styrene-isoprene triblock copolymers. *Polymer*. **104**, 279–295 (2016)
 28. I.C. Riegel, D. Samios, C.L. Petzhold, A. Eisenberg, Self-assembly of amphiphilic di and triblock copolymers of styrene and quaternized 5-(N,N-diethylamino) isoprene in selective solvents. *Polymer*. **44**(7), 2117–2128 (2003)
 29. J. Fan, C. Yu, F. Gao, J. Lei, B. Tian, L. Wang, Q. Luo, B. Tu, W. Zhou, D. Zhao, Cubic mesoporous silica with large controllable entrance sizes and advanced adsorption properties. *Angewandte Chemie Inter. Ed.* **42**(27), 3146–3150 (2003)
 30. P. Vijayan, M.A. Al-Maadeed, TiO₂ nanotubes and mesoporous silica as containers in self-healing epoxy coatings. *Sci. Rep.* **6**, 38812 (2016)
 31. A.B. Radwan, A.M. Mohamed, A.M. Abdullah, M.A. Al-Maadeed, Corrosion protection of electrospun PVDF–ZnO superhydrophobic coating. *Surf. Coatings Technol.* **289**, 136–143 (2016)
 32. H. Yang, N. Coombs, G.A. Ozin, Mesoporous silica with micrometer-scale designs. *Adv. Mat.* **9**(10), 811–814 (1997)
 33. S. Hudson, D.A. Tanner, W. Redington, E. Magner, K. Hodnett, S. Nakahara, Quantitative TEM analysis of a hexagonal mesoporous silicate structure. *Phys. Chem. Chem. Phys.* **8**(29), 3467–3474 (2006)
 34. K.M. Li, J.G. Jiang, S.C. Tian, X.J. Chen, F. Yan, *J. Phys. Chem.* **118**(5), 2454 (2014)
 35. S. Sharmiladevi, A.S. Priya, M.V. Sujitha, *Int. J. Pharm. Pharmaceut. Sci* **8**(5), 196 (2016)
 36. S.Q. Feng, Z.Y. Fu, X.Y. Shen, Y.L. Ji, Studies on the electrospun submicron fibers of SIS and its mechanical properties. *J. Appl. Polym. Sci.* **114**(3), 1580–1586 (2009)
 37. M. Bognitzki, W. Czado, T. Frese, A. Schaper, M. Hellwig, M. Steinhart, A. Greiner, J.H. Wendorff, Nanostructured fibers via electrospinning. *Adv. Mat.* **13**(1), 70–72 (2001)
 38. A. Sayari, S. Hamoudi, Periodic mesoporous silica-based organic–inorganic nanocomposite materials. *Chem. Mat.* **13**(10), 3151–3168 (2001)
 39. M. Zienkiewicz-Strzałka, M. Skibińska, S. Pikus, Small-angle X-ray scattering (SAXS) studies of the structure of mesoporous silicas. *Nucl. Instrum. Methods Phys. Res. B.* **411**, 72–77 (2017)
 40. Q. Lu, Z. Wang, J. Li, P. Wang, X. Ye, Structure and photoluminescent properties of ZnO encapsulated in mesoporous silica SBA-15 fabricated by two-solvent strategy. *Nanoscale Res. Lett.* **4**, 646–654 (2009)
 41. A.B. Abdul-Hussein, F.A. Hashim, T.R. Kadhim, *Eng. Technol. J.* **33**, 1761 (2015)
 42. A. Beganskienė, V. Sirutkaitis, M. Kurtinaitienė, R. Juškėnas, A. Kareiva, *Mat. Sci.* **10**(4), 287 (2004)
 43. K.M. Meera, R.M. Sankar, A. Murali, S.N. Jaisankar, A.B. Mandal, *Colloid. Surf. B, Biointerf* **90**, 204 (2012)
 44. H. Parangusan, D. Ponnamma, M.A. AlMaadeed, Investigation on the effect of γ -irradiation on the dielectric and piezoelectric properties of stretchable PVDF/Fe–ZnO nanocomposites for self-powering devices. *Soft Matt.* **14**(43), 8803–8813 (2018)
 45. D. Ponnamma, J. George, M.G. Thomas, C.H. Chan, S. Valić, M. Mozetič, U. Cvelbar, S. Thomas, Investigation on the thermal and crystallization behavior of high density polyethylene/acrylonitrile butadiene rubber blends and their composites. *Polym. Eng. Sci.* **55**(5), 1203–1210 (2015)
 46. Z. Xue, S. Wang, L. Lin, L. Chen, M. Liu, L. Feng, L. Jiang, A novel superhydrophilic and underwater superoleophobic hydrogel-coated mesh for oil/water separation. *Adv. Mat.* **23**(37), 4270–4273 (2011)
 47. D. Ponnamma, M. Al-Maadeed, Influence of BaTiO₃/white graphene filler synergy on the energy harvesting performance of a piezoelectric polymer nanocomposite. *Sustainable Energ. Fuel.* **3**, 774–785 (2019)
 48. S. Adham, A. Hussain, J. Minier-Matar, A. Janson, Membrane applications and opportunities for water management in the oil & gas industry. *Desalination.* **440**, 2–17 (2018)